RUHR-UNIVERSITÄT BOCHUM

RUB

Materials Research Department

No. 10 | 2013

news

Research Insights and Information

Editorial

DEAR READER,

Welcome to the 10th issue of the MRD Newsletter, which reports on research projects of MRD members from different faculties of RUB.

The MRD is closely cooperating with scientific institutions in the region, like the MPIE in Düsseldorf: the director of their new department "Structure and Nano-/Micromechanics of Materials", Prof. Dr. Dehm, is simultaneously Professor at the "Institut für Werkstoffe", Faculty of Mechanical Engineering of RUB.

This time the articles of the Newsletter share the focus on small scale materials (thin films, nanoparticles, qubits) and their mechanical, electrical and chemical properties.

An additional article reports on understanding complex intermetallic phases by atomistic simulations.

Furthermore I am happy to report that the "Institut für Werkstoffe" and "ICAMS" have moved to the new IC building and are thus now in closest vicinity on the campus (ICFO, ICFW).

Finally, the detailed planning for the new research building "ZGH" is advancing and the "Materials Days 2013" (4.–6.11.2013) will host the "International Workshop on Interface-dominated Materials", which is part of the scientific preparation for "ZGH".

Yours Sincerely,

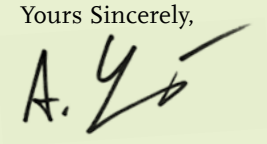

Prof. Dr.-Ing. Alfred Ludwig

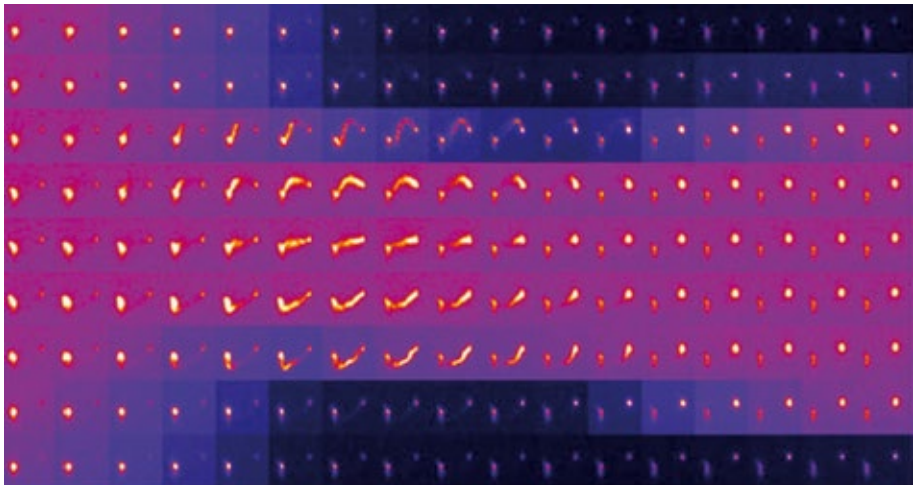

Figure 3: Composite image of (111) Laue spots of a deformed Cu single crystal bending beam. The sample was rastered by the focused synchrotron beam with a lateral resolution of 1µm. Streaked reflections indicate the presence of geometrically necessary dislocations. Image from C. Kirchlechner, M. Kapp, unpublished 2013.

Nano-/Micromechanics of Materials

The new department Structure and Nano-/Micromechanics of Materials at the Max-Planck-Institut für Eisenforschung GmbH (MPIE) aims to understand deformation mechanisms at small length scales in complex and miniaturized materials.

The mechanical challenges for structural materials applications at macroscopic length scales are apparent; while for materials employed in miniaturized systems – such as microelectronic devices or micro-electro-mechanical systems (MEMS) – the functional properties are of primary concern. However, the mechanical properties should not be overlooked as any mechanical damage may cause failure of functional devices. Frequently, the material components of functional devices/systems are exposed to extremely harsh mechanical conditions: Thin film structures for flexible electronics are cyclically bended and folded, metals and insulators in semiconductor devices are exposed to repeated thermo-mechanical loading by Joule heating or ambient temperature fluctuations, interfaces between materials of different bonding characteristics are supposed to remain intact, and miniaturized energy harvesting systems often endure aggressive chemo-mechanical environments preventing long-lasting and efficient service. To obtain quantitative mechanical data of small structures is a challenge due to the tiny material dimensions of a few micrometers or even less. However, quantitative mechanical tests are required to resolve the mechanical properties of miniaturized materials and to shed light on the deformation mechanisms which are usually altered compared to their bulk counterparts. Surfaces and interfaces impose constraining effects which need to be understood to predict the behavior of miniaturized materials and devices.

A cornerstone of the research work of the new department is the combination of quantitative and often self-build miniaturized mechanical tests with microstructure characterization techniques. This combination provides basic information on the underlying deformation mechanisms and will be illustrated in the following with a few current research examples.

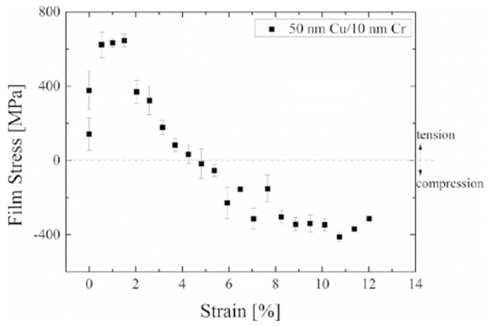

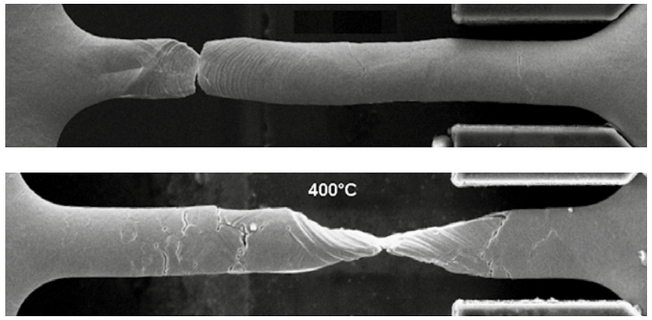

Figure 2: In situ SEM tensile test performed on freestanding polycrystalline Cu lines at (a) 25 °C and (b) 400 °C. Slip traces are resolved in some grains. (b) At 400 °C several grain boundaries start to form cracks. Images from [Smolka et al. 2012].

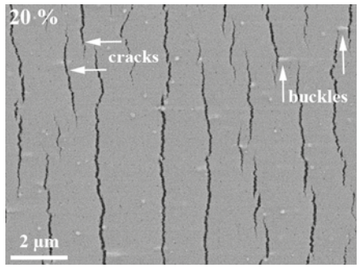

Figure 1: (a) SEM image of a 50 nm thick Cu film on polyimide strained to 20 % in tension. The SEM image reveals cracks and buckles. Buckles form due to the difference in Poission's ratio between the Cu film and the polymer. The stress evolution leading to buckling is quantified in an in situ synchrotron straining experiment. Data from V. Marx, M.J. Cordill, C. Kirchlechner, 2013 unpublished.

Fig. 1 shows a scanning electron microscopy (SEM) image of a thin metallic film on a flexible polyimide substrate, which was strained inside the SEM until fracture of the film occurred. The in situ tensile experiment reveals that lateral to the straining direction compressive stresses cause local buckling and delamination of the metallic film. Such buckles can be used to determine the "strength" of the metal-polymer interface [Cordill et al. 2010], however, without the in situ approach their existence could be overlooked as during unloading the buckles frequently vanish. Combining such a straining experiment with X-ray diffraction (XRD) provides quantitative information of the tensile and compressive stresses at which failure of the film by fracture and/or delamination occurs. Performing the tension experiment under an atomic force microscope allows determining the shape and geometry of the buckle induced delamination zone, key parameters to quantify the interface energy release rates based on mechanical models [Cordill et al. 2010].

For testing film structures independent of the substrate a lithographic process has been developed which permits to create freestanding tension samples. A commercial test rig has been modified to operate at temperatures up to 400°C inside an SEM [Smolka et al. 2012]. In that case SEM is required for accurately aligning the tension sample and the gripper and to prevent oxidation. Additionally, the in situ SEM observation resolves which grains participate in the plastic deformation by following the slip step formation at the surface of the grains (Fig. 2). Electron backscatter diffraction can be used to track orientation changes of individual grains during the deformation giving information e.g. on grain-grain interactions.

Recently, the new department at MPIE started to analyze the origin of fatigue damage in small structures by applying µLaue diffraction [Kirchlechner et al. 2012]. Bending beams of micron-sized Cu single crystals were cyclically deformed at a dedicated synchrotron beamline (Fig. 3). The µLaue pattern is sensitive to stored dislocations. Statistically stored dislocations lead to a broadening of the Laue reflections, while geometrically necessary dislocations induce an elongation of the Laue spots due to the local orientation changes created by the geometrically necessary dislocations [Barabash et al. 2009]. The in situ low cycle fatigue experiment permits to follow the formation and dissolution of dislocation pile-ups during loading and unloading, and to quantify the number of accumulated dislocations with a sub-micrometer resolution.

The above presented research examples focus on thin films and miniaturized materials. However, plasticity, fatigue, and fracture of bulk materials are initiated by local deformation processes. Thus, detecting and understanding the underlying mechanisms locally may turn out to become a key to improve the mechanical performance and lifetime not only of miniaturized materials but also of macroscopic materials.

With this short overlook I would like to present a first impression on some of our activities in the field of micromechanics of materials. Further information can be found at our homepage (see: www.mpie.de). With my adjunct professorship at the RUB and my membership in the Materials Research Department of the RUB I am looking forward to many fruitful collaborations in a research landscape which offers great opportunities to the field of materials science by multidisciplinary approaches.

Literature

1 M. J. Cordill, F.D. Fischer, F.G. Rammerstorfer, G. Dehm, Adhesion energies of Cr thin films on polyimide determined from buckling: Experiment and model, Acta Materialia, 58 (16), 2010, 5520–5531. 2 M. Smolka, C. Motz, T. Detzel, W. Robl, T. Griesser, A. Wimmer, and G. Dehm, Novel temperature dependent tensile test of freestanding copper thin film structures, Rev. Sci. Instrum. 83, (2012) 064702. 3 I. Barabash, G.E. Ice, M. Kumar, J. Ilavsky, J. Belak, Polychromatic microdiffraction analysis of defect self-organization in shock deformed single crystals, Int. J. Plast. 25, 2009) 2081. 4 C. Kirchlechner, W. Grosinge,r M.W. Kapp, P. J. Imrich, J. S. Micha, O. Ulrich, J. Keckes, G. Dehm, C. Motz, Investigation of reversible plasticity in a micron-sized, single crystalline copper bending beam by X-ray mu Laue diffraction, Philosophical Magazine, 92 (2012) 3231–3242

Prof. Dr. Gerhard Dehm
dehm@mpie.de

Generation of Nanoparticles by Laser Ablation in Liquid

Nanoparticles are more than 100 times smaller than the diameter of a human hair and due to their properties are useful in a number of applications in plasmonics, chemical reactions and biomedical engineering. The main reason for these unique properties is the large surface-to-volume ratio, which increases with decreasing particle size. There are many possibilities to synthesize nanoparticles, e.g., wet chemical sol-gel process, gas phase hydrolysis, electrochemical etching. These methods show limitations for instance in the availability of precursor materials, the processability of complex materials, the dispersion of nanoparticles, agglomeration or ability to produce pure nanoparticles without impurities and toxic chemical precursors.

Laser ablation in liquids is an effective alternative method to generate pure nanoparticles with different size parameter (1–200 nm) in a variety of liquids. Compared to laser ablation in ambient air or gas atmosphere, the generated nanoparticles in liquid environment do not agglomerate and are dispersed homogeneously after the process. Moreover, no additional chemical precursor is necessary, the chemical composition of the nanoparticles corresponds to that of the ablated target material and resulting nanoparticles are chemically pure. Further, the particle size, shape, etc. can be controlled by changing the type of liquid or laser parameters such as laser fluence, wavelength, pulse repetition rate, pulse width, etc. Fig. 1 shows a schematic of the laser ablation process in liquid media as it has been used in our experiments.

During the process, a bulk target is placed in a glass vessel which is filled by a liquid. A short (10^{-6} – 10^{-9}) or ultra-short (<0.1 ns = 10^{-10}s) laser pulse is focused on the target surface, evaporates the target and forms the nanoparticles from the clusters of vapor products of the ablated material. The laser beam can be moved by a scanner in order to increase the processed area and to decrease influence of surface inhomogenities on the generation of nanoparticles. Until today the mechanism of particle formation is not yet completely understood because the process during ablation is too fast. Generally, the main formation mechanism of generated nanoparticles consists in nucleation during the plasma plume (plasma filled with atoms, molecules, electrons, ions, clusters) and cooling followed by nuclei growth and coalescence.

Laser ablation in liquids can be also applied to fabricate nanoparticles from different materials such as Au, Ag, Ti, Ni, Fe, etc. and alloys. Jakobi et al. fabricated PtIr-NP by laser ablation in acetone and measured the material properties by scanning transmission electron microscope (STEM) and energy dispersive X-ray spectroscopy (EDX)[1], applying an ultra-short pulse laser (800 nm wavelength, 120 fs pulse duration, 300 µJ pulse energy and 5 kHz repetition rate). Lee et al. generated AuAg-NPs in water by using a Nd:YAG laser (1064 nm wavelength, 50 mJ pulse energy, 10 Hz repetition rate, 6 ns pulse duration) and detect a composition of 1:1 Au:Ag[2].

An experimental setup for the investigation of the stoichometric behavior of laser based generation of nanoparticles has been designed at the chair of Applied Laser Technology (LAT). The setup is based on a fs laser source (Amplitude System, Tangerine; P = 20 W, λ = 1030 nm, f = 100 kHz). The laser is focused on the surface of metal target (NiTi, 55.49:44.49 wt%). This material has been chosen because of the high susceptibility of the material properties on the ratio of the two elements. The target was placed in a beaker filled with one of the following liquids: water, ethanol, acetone and ethyl acetate. The total ablation time in our experiments was limited by the concentration of nanoparticles in the solvent. If the concentration is relatively high, the nanoparticles absorb the laser light, which is not advantageous while (1) the nanoparticles melt and may agglomerate and (2) less energy reaches the target surface. In earlier experiments we have revealed an effective shielding of the particle growth due to an in-situ coating with organic molecules from the surrounding liquid[3].

Barcikowski and Ostendorf et al. generated NiTi-NPs by a femtosecond laser system[4]. They characterized the materials properties and the phase transformation of the NPs by differential scanning calorimetry (DSC) and demonstrated the phase transformation of the laser-generated NPs. In this case, the behavior of an ensemble of the laser-generated nanoparticles was studied. The aim was to deposit the NPs onto an implant surface and to determine their biocompatibility by incubation of human adipose-derived stem cells (adMSCs) with NiTi-NPs.

Recently, Transmission Electron Microscopy enables analysis of the crystalline structures of individual laser-produced nanoparticles. Fig. 2 shows TEM images of NiTi-nanoparticles generated by laser ablation in water. The nanoparticles show spherical shape but in this case also a broad particle size distribution. By a special cooling holder (Gatan 636-DH), the nanoparticles were cooled and heated between –170 °C and 90 °C. At –94.9 °C a martensite phase can be detected for a diameter of around 150 nm (specifically marked in Fig. 2 a). Upon further cooling to –115.3 °C, the phase grows until fine striations of martensite twin structures are recognized (Fig. 2 b))

References

1 Jakobi, J., Menendez-Manjon, A., Sai Kiran, C.V., Lorenz, K., Wagener, P., Barcikowski, S., Nanotechnology, 2011, Vol. 22, Nr. 14, pp. 145601–145607 2 Lee, I., Han S.W., Kim, K., Chem. Commun., 2001, Vol. 18, pp. 1782–1783 3 Essaidi, A., Chakif, M., Schöps, B., Aumman, A., Xiao, S., Esen, C. and Ostendorf, A., J Laser Micro/Nanoeng., 2013, Vol. 8, Nr. 2, pp., 131–136 4 Barcikowski, S., Hahn, A., Reimers, K., Ostendorf, A., J. Nanopart. Res., 2010, Vol. 12, pp. 1733–1742

Prof. Dr. Andreas Ostendorf
Applied Laser Technology
andreas.ostendorf@rub.de

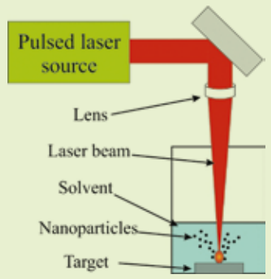

Figure 1: Schematic view of the generation of nanoparticles by laser ablation

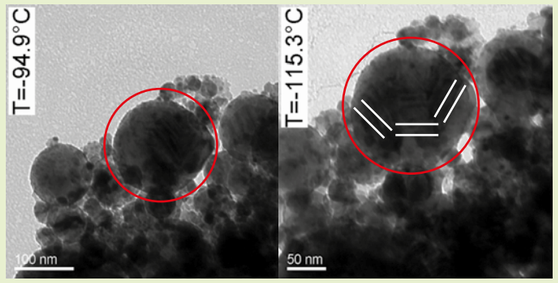

Figure 2: TEM-images of generated NiTi-NPs taken during cooling at a) T = –94.9°C and b) T = –115.3°C

Nanoscale metal oxides through chemical vapor phase approaches

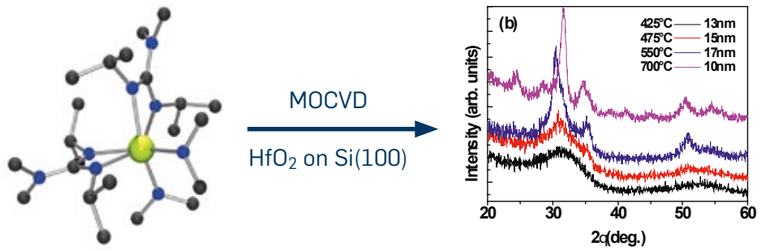

Figure 1: Molecular structure of (left) [Hf(N-Me_2)$_2$(guan)$_2$] and (right) XRD of MOCVD grown HfO_2 on Si(100), (below, left) HRTEM cross sectional view of a 7 nm thick HfO_2 film with an interlayer thickness about 2 nm and (below, right) PtSi/HfO_2/Si gate stack.

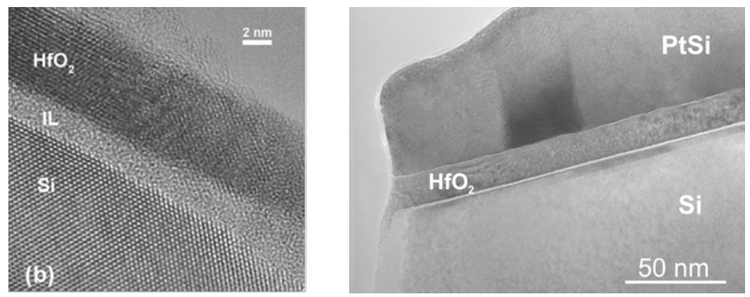

The Inorganic Materials Chemistry (IMC) research group at the Faculty of Chemistry and Biochemistry focuses on developing novel metalorganic precursors and utilizing them for the fabrication of thin films of functional metal oxides employing metalorganic chemical vapor deposition (MOCVD) and atomic layer deposition (ALD) processes. The nanostructured thin films are eventually characterized and evaluated for device applications

The general motivation for exploring precursor chemistry for group IV oxides (TiO_2, ZrO_2, HfO_2) and rare earth (RE) oxides (Y_2O_3, Sc_2O_3, Gd_2O_3, Dy_2O_3, Er_2O_3) arises from the ever increasing interest in high-quality, uniform group IV or RE containing thin films as emerging materials mainly for applications in future generation microelectronic, optoelectronic or spintronic devices. While group IV metal oxides namely, ZrO_2 and HfO_2 exhibit a wide range of functional properties which make them very promising for technological applications ranging from high dielectric constant (k) material in complementary metal oxide semiconductor (CMOS) technology to optical fibers, sensors, thermal barrier coatings waveguides etc., TiO_2 is an interesting class of material, very well investigated for several applications that include UV protection, photocatalysis, pigments, dye-sensitized solar cells etc. Rare earth (RE) oxides (e.g. Y_2O_3, Sc_2O_3, Gd_2O_3, Dy_2O_3, Er_2O_3) are very appealing for use in microelectronics, optoelectronics, magnetic devices etc.

In order to achieve high process and device integrity, there are several stringent requirements on the thin film deposition process including high miniaturization potential, precise control over the film thickness down to the sub-nanometer range, conformal coverage of complex three dimensional device geometries, combined with precise composition and film properties control. In this respect, two advanced thin film deposition techniques, MOCVD and ALD have proved over the last two decades as particularly suitable for industrial applications. Both techniques yield excellent coatings over large areas with complex surface geometry providing concomitantly a precise thickness and composition control. Apart from the some basic differences mainly related to film growth process, MOCVD and ALD have one in common and that is their strong dependence on the availability of suitable precursor chemistries. These two processes are governed by chemical reactions based on the precursors employed. Precursors are indispensable for CVD and ALD processes and over the decades, lot of developmental precursor chemistry has been carried out. In spite of the range of commonly used precursors for the growth of oxides, there are certain drawbacks associated with these compounds and therefore, over the last decade, the IMC research group in Bochum has focused on precursor engineering for MOCVD and ALD of various functional materials. The progress in terms of developing new or improved precursors and their application for some selected metal oxides (group IV and rare earth oxides), are briefly summarized within the scope of this article.

Exploratory research in the field of precursor chemistry has continued throughout the years in pursuit of improved precursors to meet the demands of emerging application for group IV oxides. In this context, the precursor development in terms of tuning group IV alkoxide and amide precursors with different chelating ligands such as ketoesters, ketoamides, malonates, ureates, carbmates, guanidinates and amidinates offer more choice for CVD and ALD applications. It was demonstrated that tiny changes in the ligand periphery of metal complexes can significantly influence the precursor properties which in turn can have a distinct bearing on the film properties[1].

The mixed alkoxides of group IV were easy to handle, dimerisation was suppressed, decomposition temperatures were lowered compared to the classical β-diketonates and the compounds were easy to synthesize and scale up[1]. The mixed amide-based complexes of group IV were volatile, less sensitive to air and moisture and thermally stable compared to their respective parent alkylamides, possess suitable reactivity for ALD applications and yielded good quality group IV oxides under the adopted MOCVD/ALD process conditions and in some selected cases tested successfully in industrial scale reactors for the growth of group IV oxides (Fig. 1).

Compared to other functional metal oxides, there are very limited reports available on the MOCVD and ALD of RE oxide thin films and this can be attributed to the lack of suitable RE precursors with appropriate physico-chemical properties

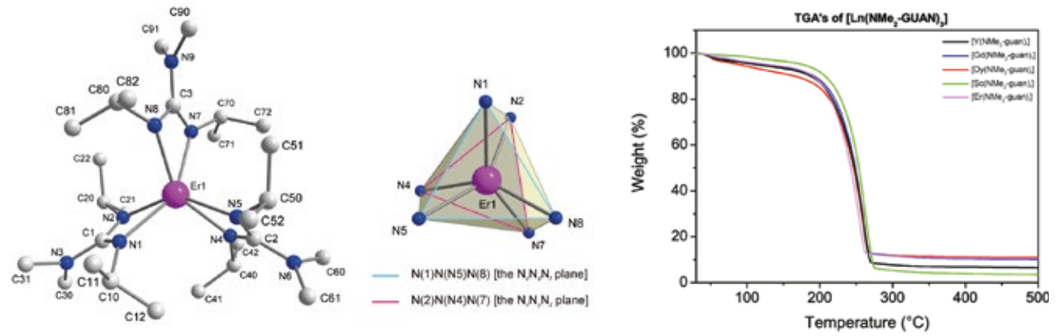

Figure 2: Molecular structure of [Er(iPr-Me_2N-GUAN)$_3$] in the solid state, (middle)Coordination polyhedron around the Er^{3+} center in [Er(iPr-Me_2N-GUAN)$_3$] and (right) Thermogravimetric analysis of RE-tris guanidinates (RE = Y, Sc, Gd, Dy, Sc).

in terms of volatility, reactivity stability and decomposition characteristics. Therefore the focus of our work was to design and develop novel RE compound classes with improved precursor-chemical properties with respect to volatility, thermal stability and suitable chemical reactivity using appropriately tailored ligand systems. For example, the N,N-dialkyl-guanidinates were selected as promising candidates[1]. The resulting RE tris-guanidinates turned out to be excellent precursors for MOCVD and ALD of RE_2O_3 thin films and can be treated as benchmark precursors for RE containing thin films (Fig. 2)[1].

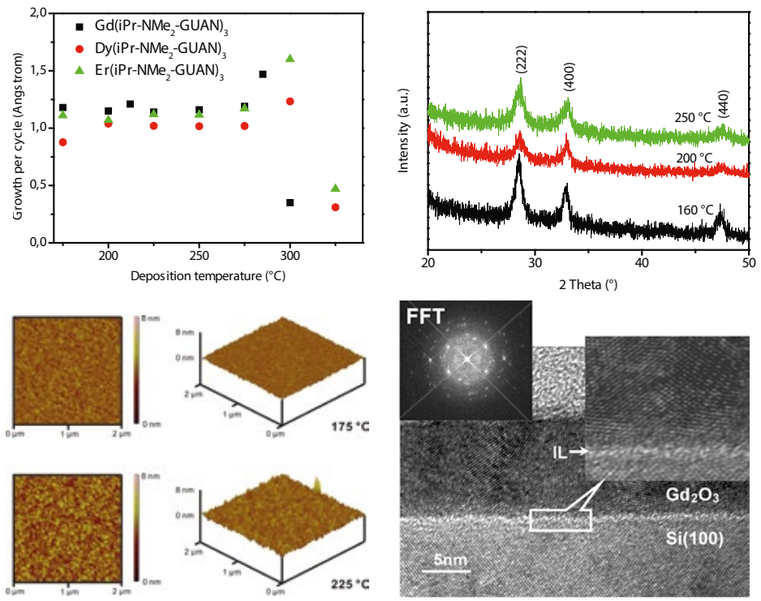

Figure 3: Water assisted ALD of RE_2O_3, RE = Gd, Dy, Er: (top, left) Growth per cycle of RE_2O_3 on Si(100) as function of substrate temperature, (top, right) XRD of Gd_2O_3 on Si(100), (below, left) AFM and (below, right) HRTEM images of Gd_2O_3 on Si(100).

Having selected the most promising candidates among the new compound classes, their suitability as precursors for MOCVD and ALD of RE oxides (Sc_2O_3, Y_2O_3, Gd_2O_3, Dy_2O_3, Er_2O_3) was successfully explored[1]. Of particular significance is the first ever demonstration of a water-assisted true ALD RE_2O_3 (Gd_2O_3, Dy_2O_3, Er_2O_3) process developed using the novel tris-guanidinato RE precursors (Fig. 3). Employing a multi-technique approach, variations of the growth characteristics and film properties with deposition temperature were studied in terms of crystallinity, structure, surface roughness, composition, and electrical properties. Device quality RE_2O_3 thin films were obtained with high growth efficiency simply by using the RE guanidinate class of precursor in combination with water and thus avoiding ozone as oxidant[1]. From the precursor engineering point of view, the idea is not only to synthesize one or more arbitrary members of a particular precursor class, rather rationally introduce small and distinct changes in the ligand sphere in a systematic manner. This is very important since such an approach would provide knowledge on the relationship between the molecular structure of the precursors, their thermal characteristics and the properties of the resulting films.

Reference:

1 A. Devi; 'Old Chemistries' for new applications: Perspectives for development of precursors for MOCVD and ALD applications, Coordination Chemistry Reviews, 2013, http://dx.doi.org/10.1016/j.ccr.2013.07.025

Prof. Dr. Anjana Devi
Inorganic Materials Chemistry
anjana.devi@rub.de

Understanding the stability of complex intermetallic phases

The design of multi-component materials requires to anticipate the crystal structures that will form during fabrication and operation. One class of complex crystal structures that are observed in many intermetallic compounds are the topologically close-packed (TCP) phases. Depending on the application, the goal of materials design with regard to TCP phases is either to enforce and control or to avoid their precipitation.

In precipitate-hardened steels, the TCP phases are used as obstacles to dislocation movement for improved creep strength. In plasma-facing alloys based on refractory metals for fusion reactors, the formation of TCP phases following nuclear transmutations may cause mechanical failure due to internal stresses on the brittle TCP phase precipitates. In Ni-base single-crystal superalloys for high-temperature applications, the TCP phases lead to a degradation of mechanical properties. A similar effect is expected for the currently developed Co-base superalloys. A more detailed understanding of the thermodynamic stability of TCP phases and their formation will therefore be beneficial for the design of the next generation of superalloys. The investigation of TCP phases in Ni-base and Co-base superalloys is one of the common aims of experimental and theoretical projects in the SFB/Transregio 103 From Atoms to Turbine Blades – A Scientific Approach for Developing the Next Generation of Single Crystal Superalloys.

In order to gain a microscopic understanding of the stability-determining factors, we carry out atomistic simulations based on the electronic structure. We use a hierarchy of simulation methods that treat the electronic structure at different levels of coarse-graining, i.e. at different levels of computational cost and accuracy. In particular, we compute the formation energy of TCP phases with density-functional theory (DFT), with tight-binding (TB) and with bond-order potential (BOP) calculations that provide a physically intuitive and local interpretation of interatomic interactions.

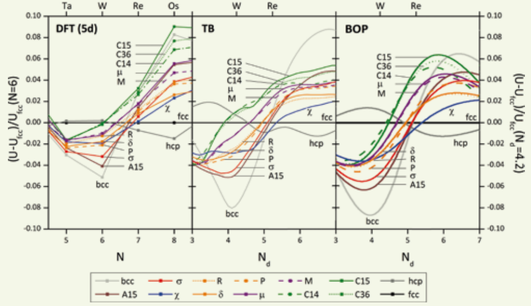

The key to understanding the structural stability of the TCP phases is their crystallography. The crystal lattices of the TCP phases (A15, σ, χ, P, R, δ, μ, M and Laves phases C14, C15 and C36) are characterized by the presence of a limited number of distinct Frank-Kasper coordination polyhedra (Fig. 1). These polyhedra differ by the coordination number (i.e. the number of nearest neighbors) of the central atom ranging from 12 to 16. The combination of polyhedra with different coordination number causes a relation between their different volume in the crystal lattice and the volume of the atoms that occupy the different crystal sites. This leads to an influence of atomic-size differences ΔV/V on the structural stability in multi-component systems. The translational symmetry of the lattice and the internal degrees of freedom lead to distortions of the perfect Frank-Kasper coordination polyhedra. The difference in the degree of distortion is reflected in dissimilar bond lengths and angles. This leads to modifications in the electronic structure and creates an influence of the number of electrons on the trends in structural stability. In a multi-component system this influence depends only on the average valence-electron concentration N which reduces the modelling complexity to feasibility. The interplay of both contributions to the structural stability is reflected in the chemical composition of experimentally observed TCP phases.

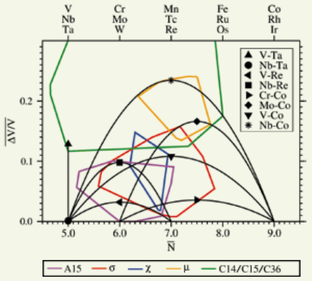

We could pinpoint the influence of N on structural stability by showing that the TCP phases form several groups of similar stability, namely C14/C15/C36, μ/M, R/P/δ, as well as σ/A15/χ on all coarse-graining levels of our simulation techniques (Fig. 2). On the level of BOP calculations this grouping can be directly attributed to the bimodality of the electronic density of states caused by distortions of the local coordination polyhedra mentioned above. We also confirm the experimentally observed sequence of A15→σ→χ with increased average valence-electron concentration at the transition from a body-centered cubic to a face-centered cubic crystal structure at the center of the transition-metal series. This also explains the finding that TCP phase precipitates in superalloys contain high local concentrations of refractory elements that were added to increase the creep resistance (Mo, Re, W) and to retard the coarsening of the γ' phase (Re). The Laves phases C14/C15/C36 are rather high in energy, which demonstrates that additional contributions from ΔV/V are required to stabilize them.

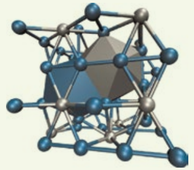

The effect of atomic-size differences and the interplay with the average valence-electron concentration can be understood by matching high-throughput DFT calculations with an empirical structure map. The latter casts the experimentally observed TCP phases in regions based on the values of N and ΔV/V for the corresponding chemical compositions (Fig. 3). The DFT calculations are carried out for TCP phases in selected binary systems and allow us to assess the complex interplay of both structure-stabilizing factors for different values of N and ΔV/V. In collaborations within the SFB/Transregio 103 the structure map is also used to anticipate which TCP phase is formed given the local chemical compositions from EPMA measurements.

The combination of atomistic simulation methods at different levels of coarse-grained electronic structure with structure maps based on experimental observations provide a powerful toolbox for understanding and predicting the formation of complex intermetallic phases in multi-component systems. We believe that these modelling techniques and the close links to experimental projects, particularly in the SFB/Transregio 103, will contribute to the understanding and development of new alloys. Our ongoing development of 3-dimensional structure maps make us optimistic that the prediction of crystal structures for compound systems can be applied to a much broader scope.

Dr. Thomas Hammerschmidt
Department of Atomistic Modelling and Simulation, ICAMS

Semiconductor material for electrical control of a solid-state flying qubit

In contrast to current binary bits, which are based on electrical charge or the corresponding voltage, future information processing will be based on quantum bits (qubits) which include the electron spin and its orientation. They must be able to be integrated in the current main-stream microtechnology. That is why, solid-state approaches to quantum information technology are attractive: They are scalable. The coherent transport of quantum information over large distances is a requirement for any practical quantum computer and has been demonstrated by coupling superconducting qubits to photons[1]. Single electrons have also been transferred between distant quantum dots in times shorter than their spin coherence time[2,3]. However, until now, there have been no demonstrations of scalable 'flying qubit' architectures – systems in which it is possible to perform quantum operations on qubits while they are being coherently transferred – in solid-state systems. These architectures allow for control over qubit separation and for non-local entanglement, which makes them more amenable to integration and scaling than static qubit approaches. Here, we report the transport and manipulation of qubits over distances of 6 μm within 40 ps, in an Aharonov-Bohm (AB) ring connected to two channel wires that have a tunable tunnel coupling between the channels. The electric conductive part of this AB-ring is made of a 2-dimensional electron gas (2DEG), embedded in an $Al_{0.3}Ga_{0.7}As$-GaAs heterostructure grown by molecular beam epitaxy (MBE) at the Ruhr-University in Bochum (Fig. 1).

The whole structure is depicted in Fig. 2: By laterally structured, finger-shaped top gates, the 2DEG is depleted underneath them, leaving only the 2DEG areas in between them conductive. In this way, the wires and thus the whole AB-ring is built up. In addition, the wires before and after the AB-ring are very close to each other, only being separated by a narrow, bias-adjustable finger gate in between them. It is thus possible to swap the electron motion from one wire to the other both at the entrance and at the outlet of the AB-ring. The flying qubit state is defined by the presence of a travelling electron in either channel of the wire, and can be controlled without a magnetic field. Our device has shorter quantum gates (<1 μm), longer coherence lengths (~86 μm at 70 mK) and higher operating frequencies (~100 GHz) than other solid-state implementations of flying qubits[4,5]. The flying qubit device described here is an electrical analogue of an optical two-path interferometer, in which the qubit basis is defined by the presence of a travelling electron in either of the two paths. Similar electrical two-path interference has been achieved in Mach-Zehnder interferometers of quantum Hall edge channels[4,5], which have been the testing grounds for quantum physics such as orbital entanglement[6,7]. However, these devices exhibit edge-channel coherence lengths of 24 μm at 20 mK (ref. 5). This, together with a requirement for high magnetic fields, limits their scalability. Compared with edge-channel two-path interferometers, our two-path interferometer operates at a lower magnetic field, has well defined quantum operations, shorter quantum gates and longer coherence lengths. Despite its apparent simplicity, the realization of such an electrical two-path interferometer at low magnetic fields is highly challenging. The main difficulty comes from the nature of the electrons on the Fermi surface – electrons usually take multiple paths, so the quantum phase of an electron is easily scrambled. This causes the quantum information being carried by the electron to be lost. Electrons travelling through an Aharonov-Bohm (AB) interferometer[8-11], generally known as a two-path interferometer, also suffer from the existence of multiple paths. Electron interference arises in AB interferometers due to the phase the electron acquires in one path relative to the other, with the phase difference being given by $\Delta\varphi = \oint k\,dl - (e/\hbar)\,BS$. Here, B is the perpendicular magnetic field and S is the area enclosed by the AB ring. This phase difference causes an oscillation of the current as a function of B with a period of $\hbar/\Upsilon_S$. It turns out, however, that the two terminal linear conductance through an AB ring suffers from so-called phase rigidity[12-14]. Onsager's law for linear conductance[12,15,16], G(B) = G(–B), implies that the phase of the AB oscillation can take only the values 0 or π at B = 0. To satisfy this boundary condition imposed by the contact geometry while still allowing for a continuous phase variation Δφ, contributions from multiple scattered paths need to be added to Δφ. What is usually observed in an AB experiment is therefore not an ideal two-path interference, but a complicated multipath interference. Such conventional AB interference is shown in Fig. 2b,c. Multi-terminal devices have also been used to extract the contribution of the two path interference and avoid phase rigidity[17]. However, the multipath contribution is still present even in such interferometers, and leads to the loss of quantum information carried by coherent electrons reaching other reservoirs. Here, we realize a novel two-path interferometer that can act as a flying qubit by combining the AB ring with two-channel wires, that is, parallel tunnel-coupled quantum wires[18,19] that allow tunnelling of an electron between the two paths (Fig. 2 and 3). We define the two pseudo spin states |↑> and |↓>, where |↑> and |↓> correspond to the state having an electron in the upper and lower path, respectively[20-22]. In such a structure, any superposition state of |↑> and |↓> in the ring can transmit into the tunnel-coupled wire by being directly transformed into the super position of the bonding and antibonding state in the tunnel-coupled wire, that is, $\Psi_S = (1/\sqrt{2})(|\uparrow\rangle + |\downarrow\rangle)$ and $\Psi_{AS} = (1/\sqrt{2})(|\uparrow\rangle - |\downarrow\rangle)$ This is in contrast with the conventional AB ring with only single wire leads, where only cS is transmitted into the leads. Consequently, this new structure works as a two path interferometer for ballistic electrons, which does not suffer from paths encircling the AB ring due to the absence of backscattering at the entrance of the tunnel coupled wire. The pseudo spin is then defined as a flying qubit. It is important to mention that even though the electron wave spreads over the interferometer under low-energy excitation, the pseudo spin state is explicitly defined at each position in the interferometer. Therefore, a flying qubit state carried by each single electron is strictly defined as a function of the position without uncertainty. Our device (Fig. 2a) is defined by surface Schottky gates on a two-dimensional electron gas at the interface of a high-mobility GaAs/AlGaAs heterostructure. The negative gate voltages V_{T1} and V_{T2} applied on the orange-coloured central gates allow control of the tunnel coupling between the upper and lower paths. Because these gates are as narrow as 50 nm at the tunnel-coupled regions, the tunnel coupling at the right coupled wire can be kept sufficiently strong, even when the central region of the device is depleted by V_{T1} to form an AB ring. The side gates of the AB ring, V_{M1} and V_{M2}, allow for modulation of the Fermi wave vectors in the ring. All measurements except those in Fig. 4 were carried out in a dilution refrigerator at T = 70 mK. The initial qubit state is simply defined as |↑> by injecting electrons into only one of the two wires. The projection of the final state is obtained by measuring the output currents, $I_\uparrow$ and $I_\downarrow$. Tunnel coupling between the two wires yields the hybridized symmetric and antisymmetric basis states, Ψ_S and Ψ_{AS}, with confinement energies E_S and E_{AS}, respectively. The energy spacing $\Delta E = E_{AS} - ES$ is given by the tunnel coupling energy. The quantum state of an electron wave, which is a superposition state of Ψ_S and Ψ_{AS}, then acquires a relative phase $\vartheta = (1/\hbar)\Delta E\tau$ between Ψ_S and Ψ_{AS}, where $t \approx L_t/v_F$ is the traversal time for electrons propagating over the length L_t of the tunnel coupling with Fermi velocity vF. ϑ is the rotation angle of a state vector about the x-axis on the so called Bloch sphere (Fig. 4). This rotational operator is expressed as the matrix in Fig. 4.

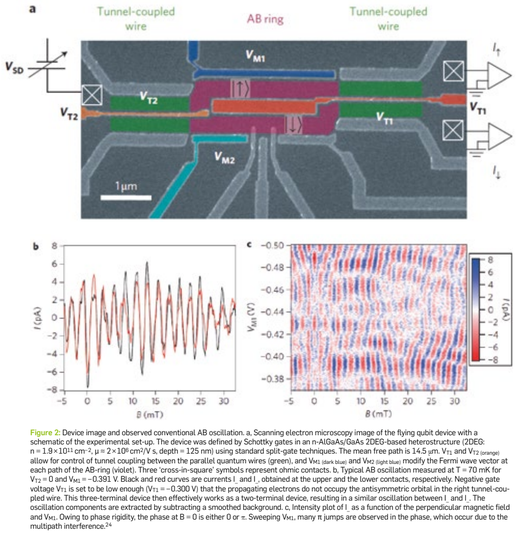

Figure 2: Device image and observed conventional AB oscillation. a, Scanning electron microscopy image of the flying qubit device with a schematic of the experimental set-up. The device was defined by Schottky gates in an n-AlGaAs/GaAs 2DEG-based heterostructure (2DEG: $n = 1.8\times10^{11}$ cm^{-2}, $\mu = 2\times10^6$ cm^2/V s, depth = 125 nm) using standard split-gate techniques. The mean free path is 14.5 μm. V_{T1} and V_{T2} (orange) allow for control of tunnel coupling between the parallel quantum wires (green), and V_{M1} (dark blue) and V_{M2} (light blue) modify the Fermi wave vector at each path of the AB-ring (violet). Three 'cross-in-square' symbols represent ohmic contacts. b, Typical AB oscillation measured at T = 70 mK for $V_{T2} = 0$ and $V_{M1} = -0.391$ V. Black and red curves are currents $I_\uparrow$ and $I_\downarrow$ obtained at the upper and the lower contacts, respectively. Negative gate voltage V_{T1} is set to be low enough ($V_{T1} = -0.300$ V) that the propagating electrons do not occupy the antisymmetric orbital in the right tunnel-coupled wire. This three-terminal device then effectively works as a two-terminal device, resulting in a similar oscillation between $I_\uparrow$ and $I_\downarrow$. The oscillation components are extracted by subtracting a smoothed background. c, Intensity plot of $I_\uparrow$ as a function of the perpendicular magnetic field and V_{MI}. Owing to phase rigidity, the phase at B = 0 is either 0 or π. Sweeping V_{M1}, many π jumps are observed in the phase, which occur due to the multipath interference.[14]

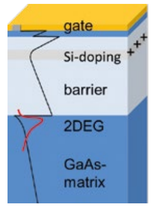

Figure 1: Cross-section of a $Al_{0.3}Ga_{0.7}As$-GaAs hetero-structure with the slope of the conduction band (black line, energy scale to the right) and the wave function of the 2DEG (red line, square of the absolute wave function to the right). The GaAs-substrate("matrix") is dark blue, the $Al_{0.3}Ga_{0.7}As$-barrier layer with the higher bandgap is light blue. The mobile elecrons in the 2DEG are separated from their mother donors (Si-doping) which allows for a very high electron mobility at low temperatures. The top Schottky gate (yellow) is able to deplete the 2DEG by a negative voltage, typically below –3V (drawing courtesy of Arne Ludwig, RUB).

means that there is basically no backscattering for the oscillating signal transmitted through the tunnel-coupled wire. The anti-phase oscillations are therefore evidence of the oscillation of the electron between the two wires, induced by tunnel coupling. Here the visibility of the oscillation, the ratio of the oscillation component to the total current, is limited to ≈ 1 %. This is due to the existence of a few transmitting channels and the high measurement temperature. Note that at low temperatures (much lower than T = 2.2 K), disorder scattering in the quantum wires leads to complicated fluctuations of the output currents as a function of V_{T1}, which masks the current oscillation induced by tunnel coupling. A rotation about the z-axis can be achieved in the AB ring by varying the magnetic field or the gate voltages V_{M1} and V_{M2} (Fig. 5).

Corresonding to the rotational matrix operators $R_x(\theta)$ and $R_z(\varphi)$ depicted in Fig. 4 and 5 about the x- and z-axis on the Bloch sphere, we measure thus in direct electronic transport the quantum mechanical states: The combination of R_x and R_z enables the generation of an arbitrary vector state on the Bloch sphere. Arbitrary rotation of the state is also possible by simultaneously controlling the tunnel coupling and the difference of the transmission phase between the two paths.

These results therefore demonstrate ideal two-path interference with no phase rigidity, and the qubit can be controlled even without a magnetic field. The flying qubit presented here is promising for quantum information technology. In addition to the ability to transfer the quantum information over a long distance, it has a much shorter operation time compared with other qubits in solid-state systems. The operation time L/v_F (L, gate length; v_F, Fermi velocity) is of the order of 10 ps. This flying qubit can also be used in combination with a static qubit [23]. Using a high-mobility heterostructure with a mean free path exceeding 100 μm, we would in principle be able to integrate 100 qubits because each quantum operation, including two-qubit operation, is performed within a 1 μm scale.

The author is indebted to his coauthors Michihisa Yamamoto, Shintaro Takada, Christopher Bäuerle, Kenta Watanabe, and Seigo Tarucha in Ref. 24 who made the whole story possible and thus configured with him wide parts of this article.

Prof. Dr. Andreas D. Wieck
Applied Solid State Physics
andreas.wieck@rub.de

Figure 3: Schematical representation of the electron's tunnel-swapping from one state to the other (green areas in Fig. 2a): The pseudospin-state |↑> tunnels to |↓>.

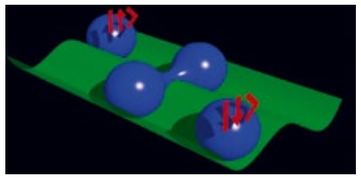

Figure 4: Demonstration of R_x operation. **a** Evolution of the flying charge qubit state via tunnel coupling. **b** Measured output currents in the tunnel-coupled wire. There are at least three transmitting modes in each wire. Black and red curves are the output currents I↑ and I↓ measured as a function of gate voltage V_{T1} for $V_{sd} = 50\,\mu V$, $V_{T2} = -0.84$ V and T = 2.2 K when the current is injected from the upper wire. Blue and green curves are measured output currents I↑ and I↓ when the current is injected to the lower wire with the same gate voltage configuration. Coincidences between the black and green curves and between the red and blue curves indicate that the oscillation of the current is due to tunnel coupling between the two paths. Note that the measurement of the current at the relatively high temperature of T = 2.2 K does not suffer from universal conductance fluctuations originating from disorder. **c** Oscillating, π-phase shifted components of the output currents. Smoothed backgrounds are subtracted from the black and red curves of **b**.[24]

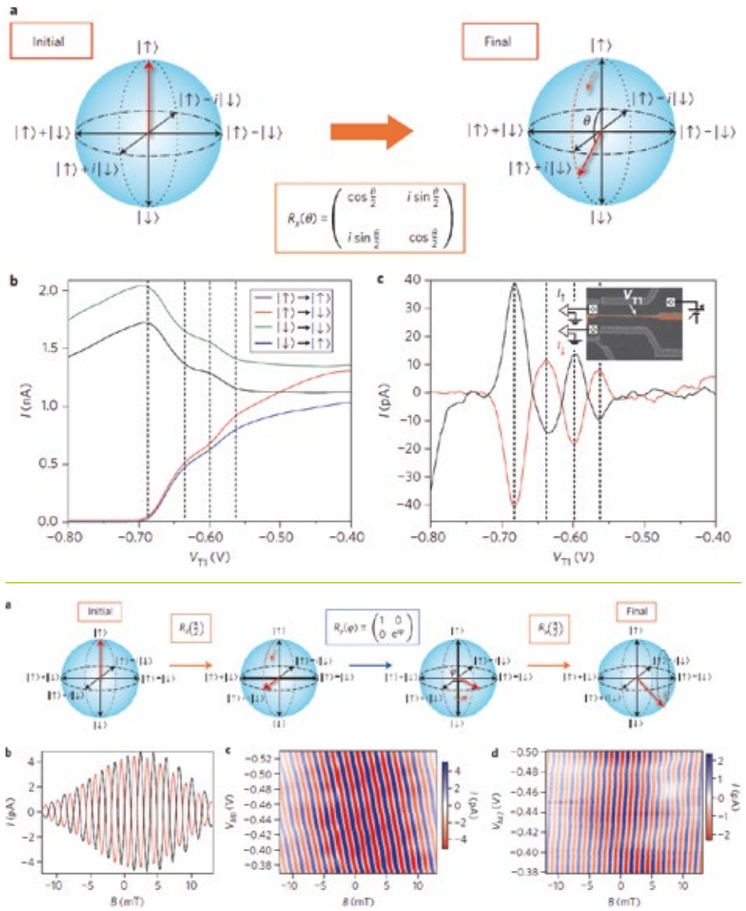

Figure 5: Demonstration of R_z operation. **a** Evolution of the flying qubit state in the scheme of the so called Ramsey interference. **b** Output current oscillation as a function of magnetic field. Black and red curves are output currents I↑ and I↓, respectively, measured for $V_{sd} = 50\,\mu V$. Both tunnel-coupled wires work as $R_x(\pi/2)$, which results in maximum current oscillation. **c** Intensity plot of I↑ as a function of magnetic field B and side gate voltage V_{M1}. **d** Intensity plot of I↑ as a function of B and V_{M2}. The oscillation components are extracted by a Hamming window followed by a fast Fourier transform filter for **b** – **d**. In both **c** and **d**, there is no phase jump of π, in contrast to Fig. 2c, which is a proof of the two-path interference.[24]

References

1 Wallraff, A. et al. Strong coupling of a single photon to a superconducting qubit using circuit quantum electrodynamics. Nature 431, 162–167 (2004). 2 Hermelin, S. et al. Electrons surfing on a sound wave as a platform for quantum optics with flying electrons. Nature 477, 435–438 (2011). 3 McNeil, R. et al. On-demand single-electron transfer between distant quantum dots. Nature 477, 439–442 (2011). 4 Ji, Y. et al. An electronic Mach-Zehnder interferometer. Nature 422, 415–418 (2003). 5 Roulleau, P. et al. Direct measurement of the coherence length of edge states in the integer quantum Hall regime. Phys. Rev. Lett. 100, 126802 (2008). 6 Samuelsson, P., Sukhorukov, E.V. & Büttiker, M. Two-particle Aharonov-Bohm effect and entanglement in the electronic Hanbury Brown-Twiss setup. Phys. Rev. Lett. 92, 026805 (2004). 7 Neder, I. et al. Interference between two indistinguishable electrons from independent sources. Nature 448, 333–337 (2007). 8 Aharonov, Y. & Bohm, D. Significance of electromagnetic potentials in the quantum theory. Phys. Rev. 115, 485–491 (1949). 9 Washburn, B.S. & Webb, R.A. Aharonov–Bohm effect in normal metal quantum coherence and transport. Adv. Phys. 35, 375–422 (1986). 10 Tonomura, A. et al. Observation of Aharonov–Bohm effect by electron holography. Phys. Rev. Lett. 48, 1443–1446 (1982). 11 Giesbers, A.J.M. et al. Correlation-induced single-flux-quantum penetration in quantum rings. Nature Phys. 6, 173–177 (2010). 12 Onsager, L. Reciprocal relations in irreversible process. Phys. Rev. 38, 2265–2279 (1931). 13 Yeyati, A.L. & Büttiker, M. Aharonov-Bohm oscillations in a mesoscopic ring with a quantum dot. Phys. Rev. B 52, R14360–R14363 (1995). 14 Yacoby, A., Schuster, R. & Heiblum, M. Phase rigidity and h/2e oscillations in a single-ring Aharonov–Bohm experiment. Phys. Rev. B 53, 9583–9586 (1996). 15 Büttiker, M. Four-terminal phase-coherent conductance. Phys. Rev. Lett. 57, 1761–1764 (1986). 16 Benoit, A. D., Washburn, S., Umbach, C. P., Laibowitz, R. B. & Webb, R. A. Asymmetry in the magnetoconductance of metal wires and loops. Phys. Rev. Lett. 57, 1765–1768 (1986). 17 Schuster, R. et al. Phase measurement in a quantum dot via a double-slit interference experiment. Nature 385, 417–420 (1997). 18 Del Alamo, J. A. & Eugster, C. C. Quantum field-effect directional coupler. Appl. Phys. Lett. 56, 78–80 (1990). 19 Tsukada, N., Wieck, A. D. & Ploog, K. Proposal of novel electron wave coupled devices. Appl. Phys. Lett. 56, 2527–2529 (1990). 20 Bertoni, A., Bordone, P., Brunetti, R., Jacoboni, C. & Reggiani, S. Quantum logic gates based on coherent electron transport in quantum wires. Phys. Rev. Lett. 84, 5912–5915 (2000). 21 Ionicioiu, R., Zanardi, P. & Rossi, F. Testing Bell's inequality with ballistic electrons in semiconductors. Phys. Rev. A 63, 050101(R) (2001). 22 Yu, L. & Voskoboynikov, O. Ballistic Aharonov-Bohm quantum bits and quantum gates. Solid State Commun. 145, 447–450 (2008). 23 Schomerus, H. & Robinson, J.P. Entanglement between static and flying qubits in an Aharonov-Bohm double electrometer. New J. Phys. 9, 67 (2007). 24 M. Yamamoto et al., Nature Nanotechnology 7, 247–251 (2012).

Short News

Meeting of the DGM Regional-forum Rhein-Ruhr on 5. and 6. September 2013 in Bochum

The DGM (Deutsche Gesellschaft für Materialkunde) is the German national scientific society for researchers and developers from industry and academia in the area of materials science and technology. Recently, DGM members have started to create local DGM centers, referred to as "DGM Regionalforen". During the annual DGM day 2013, which was held in May at the Ruhr-Universität Bochum, a new DGM Regionalforum Rhein-Ruhr was founded with Gunther Eggeler as its first speaker. All universities and research institutes from the wider Ruhr area with a research focus on materials science and engineering participate in the activity. Members come from RWTH Aachen, Ruhr-Universität Bochum, Universität Duisburg Essen, MPI für Eisenforschung, Universität Paderborn, DLR Köln, Universität Siegen, TU Dortmund and FZ Jülich.

The photograph shows members of the Regionalforum Rhein-Ruhr at their first meeting which was held on 5/6th September at the Horst Görz Saal in the Technology Center close to the Ruhr-Universität Bochum. One objective of the meeting was to discuss microstructure based materials design. Another objective was to present the activities of all partners in materials education and research. At their first meeting the partners agreed on how to run the Regionalforum Rhein-Ruhr. Especially it was agreed to invite other partners to participate in events like lecture series and symposia. The dates and locations for the next two annual meetings were agreed upon (4./6. September 2014: FZ Jülich – Materials and energy, 3./4. September 2015: Universität Siegen – Materials for light weight structures). Most importantly, the DGM Regionalforum Rhein-Ruhr aims at providing a platform for discussing ideas, developing new research strategies and to strengthen the solidarity between materials researchers in a competitive environment. The MRD of the Ruhr-Universität Bochum fully supports the activities of the DGM Regionalforum Rhein-Ruhr.

EU funds RAPID – Marie-Curie Initial Training Network at Ruhr University Bochum

The European Union has granted about 3.9 Mio. Euros for 'RAPID' a Marie-Curie Initial Training Network for a funding period of 4 years starting October 2013. RAPID (Reactive Atmospheric Plasma processIng – eDucation network) is an interdisciplinary initial training network (ITN) at the intersection of chemistry, physics and engineering aimed particularly at the development of non-equilibrium reactive processes in atmospheric pressure plasmas. Thereby, the great success of low-pressure plasmas enabling a multitude of applications ranging from material synthesis, automotive and microelectronics can be repeated. This research and training is coordinated by the Ruhr University Bochum (RUB), Germany, and will be accomplished in a consortium involving 10 academic and 10 industrial partners from 8 European countries. For more details: www.rapid-itn.eu

Prof. Dr. Achim von Keudell
Research Group Reactive Plasmas
Faculty of Physics and Astronomy
Achim.vonKeudell@rub.de

Prof. Dr. Anjana Devi
Inorganic Materials Chemistry
Faculty of Chemistry and Biochemistry
anjana.devi@rub.de

Materials Research Department

If you wish to receive this newsletter regularly or wish to unsubscribe, please send an email to **mrd@rub.de**

IMPRESSUM

Publisher:
Materials Research Department
Ruhr-Universität Bochum

Contact:
Ruhr-Universität Bochum
Materials Research Department
Prof. Dr.-Ing. Alfred Ludwig
Universitätsstraße 150
D-44801 Bochum
Building ICFO, Floor 03, Room 225
Tel.: +49 (0)234 / 32-27492
Fax: +49 (0)234 / 32-14409
E-Mail: mrd@rub.de
Web: www.rub.de/rd/mrd

Design:
jungepartner.de

RUHR UNIVERSITÄT BOCHUM RUB